

## Article

# Fast Elemental Analysis of Heavy Mineral Suites by Scanning Electron Microscopy (SEM-Unity BEX)

Jim Buckman <sup>1,\*</sup> , Amy Gough <sup>1</sup>  and Max Webb <sup>2</sup>

<sup>1</sup> Institute of GeoEnergy Engineering, School of Energy, Geoscience, Infrastructure and Society, Heriot-Watt University, Edinburgh EH14 4AS, UK; a.gough@hw.ac.uk

<sup>2</sup> The Lyell Centre, Heriot-Watt University, Edinburgh EH14 4AS, UK; max.webb@hw.ac.uk

\* Correspondence: j.buckman@hw.ac.uk

**Abstract:** Developments in scanning electron microscopy (SEM) have introduced instant live coloured SEM images based on elemental composition. Here, we use a technique utilising a Unity BEX detector system, with collection speeds up to 100 times faster than typical standard energy-dispersive X-ray (EDX) analysis systems, to obtain large area backscattered and elemental composition maps of heavy mineral (HM) suites from a sample from an Oligocene fluvio-deltaic system in the Central Myanmar Basin. The fast X-ray collection rate and a high-resolution backscattered (BSE) detector allow for rapid imaging of polished blocks, thin sections, and stubs. Individual HM species can be rapidly classified, allowing for the subsequent collection of compositional and morphological metrics. In addition, the identification of grains such as zircon and apatite allow for further analysis by cathodoluminescence (CL) to identify and record the presence of growth zonation, which is critical for further U-Pb geochronology and thermochronology, using fission track analysis of apatite, zircon, and titanite. The sample used in this study contains a diverse heavy mineral suite due to the complex tectonic history of Myanmar, juxtaposing multiple metamorphic basement terranes alongside volcanic arcs and obducted ophiolites. This, along with the textural and mineralogical immaturity of the sediments themselves (governed by short transport systems and the rapid weathering of the sources), means that a wide variety of heavy mineral species can be identified and tested using this new technique, which provides a time-efficient method in comparison to traditional optical techniques. As the Unity BEX detector is located at the polepiece, it is relatively insensitive to working distance; in addition, the geometry of paired X-ray detectors on either side of the polepiece (at 180°) means that the system is also capable of fully characterising individual particles, on uncut and unpolished grain mounts, without artefacts such as particle shadowing. The development of a more comprehensive heavy mineral EDX database (library) will improve the accuracy of this new technique, as will the correlation with other techniques such as Raman spectroscopy.

**Keywords:** automation; rapid mapping; heavy minerals; BEX



**Citation:** Buckman, J.; Gough, A.; Webb, M. Fast Elemental Analysis of Heavy Mineral Suites by Scanning Electron Microscopy (SEM-Unity BEX). *Minerals* **2024**, *14*, 950. <https://doi.org/10.3390/min14090950>

Academic Editors: Teresa Pereira da Silva, Daniel P. S. De Oliveira and João Pedro Veiga

Received: 16 August 2024

Revised: 13 September 2024

Accepted: 16 September 2024

Published: 19 September 2024



**Copyright:** © 2024 by the authors. Licensee MDPI, Basel, Switzerland. This article is an open access article distributed under the terms and conditions of the Creative Commons Attribution (CC BY) license (<https://creativecommons.org/licenses/by/4.0/>).

## 1. Introduction

Heavy minerals (HM) are those with a density greater than 2.8 to 2.9 g/m<sup>3</sup> [1] and commonly form around 1% of siliciclastic sediments. They are particularly useful in provenance studies [2–4] and can provide additional information on weathering, sediment transport, sediment mixing, and the degree of sediment recycling [3,5,6]. In such cases, heavy mineral species are typically paired (e.g., apatite/tourmaline (ATi), garnet/zircon (GZi), rutile/zircon (Ru/Zi) monazite/zircon (MZi) and chrome spinel/zircon (CZi)) and used as indexes for provenance, weathering, transportation, and degree of diagenetic alteration [7]. They also provide a method for dating sediment sources through the separation and study of mineral phases such as zircon and apatite [8–11] using SHRIMP or LA-ICP-MS U-Pb geochronology and fission track analysis [12–14]. Additionally, in some cases, high

concentrations of HMs can be mined as valuable reserves of critical metals such as Nb, Ta, Sn, Zr, and Ti [15,16].

Due to the relative scarcity of heavy minerals in sediment, they normally require separation and concentration [16–19] and are traditionally sorted, hand-picked, and identified using optical microscopy [20–22]. The latter is time-consuming and requires a specialised knowledge of mineral optical properties. In recent years, it has been identified that optical analysis can produce varied results and occasionally introduce operator bias [23], which techniques for automated mineralogy can reduce. Combined SEM-EDX has been employed in the characterisation and composition of HM phases [15,17], which has included the use of automated SEM-EDX analysis using QEMSCAN [24], as well as more novel applications with machine learning applied to HM SEM-EDX data [25]. Other authors have used Raman spectroscopy [3,9,26,27] and ICP-AES [21].

Here, we illustrate a fast and efficient method that utilises SEM and BEX (combined backscattered electron and X-ray). This method can quickly collect high-resolution images (for size, shape, and distribution of heavy minerals) at the same time as elemental composition data. Once collected, data such as spatial distribution can be further extracted and used as the basis of additional analysis for Raman spectroscopy, cathodoluminescence, microprobe studies, and ICP analysis. The pros and cons of this technique are discussed, as are potential future improvements that would make automated HM analysis a valuable routine method.

## 2. Materials and Methods

The sample heavy mineral separate utilised herein was collected from the Oligocene fluvio-deltaic Padaung Formation from the Central Myanmar Basin (MCM-18-004). The Central Myanmar Basin (Figure 1) is an elongate basin containing ~15 km of Cenozoic sediment; it is bound by the Sino-Myanmar ranges (Jurassic to Eocene medium- to high-grade metamorphic rocks) in the east and the Indo-Myanmar ranges (Triassic to Eocene schists, turbidites, and ophiolitic rocks) in the west [9].

The methodology is illustrated in the form of a flow chart (Figure 2) and follows standard mineral separation processes [16–19,28]. Five hundred grams of medium-grained sandstone were partially disaggregated using a mortar and pestle before being milled using a Fritsch Pulverisette tungsten carbide mill (Fritsch, Idar-Oberstein, Germany) with a plate separation of 0.10 mm. The loose sediment was then sieved to a 63  $\mu\text{m}$  to 250  $\mu\text{m}$  fraction using a Fritsch Analysette 3 Spartan wet sieve (Fritsch, Idar-Oberstein, Germany) and cleaned using a sodium hexametaphosphate solution combined with sonic agitation. This 63  $\mu\text{m}$  to 250  $\mu\text{m}$  aliquot was then hydrodynamically separated into light, intermediate, and heavy fractions using a Holman–Wilfley 800 Laboratory Table (Holman–Wilfley, Redruth, UK) set to an angle of 15° with low amplitude vibrations. The retained heavy mineral fraction underwent an acetic acid bath to remove any carbonate content before using a hand magnet to remove any highly magnetic minerals. Eighty grams of the remaining sample was then separated using lithium heteropolytungstate (LST), a heavy liquid with a density of  $2.89 \pm 0.02$  g/mL, to separate the heavy minerals. The concentrated HM separate was embedded into pucks using Araldite AY 103 resin and HY 956 hardener (Huntsman Advanced Materials, The Woodlands, TX, USA) and hand-polished for bulk SEM elemental analysis. In addition, individual HM grains were mounted onto a standard aluminium SEM stub to observe phases in their natural states. Both sample types were coated in gold, using an Emitech K550 gold sputter coater (Emitech Ltd., Ashford, UK), and analysed in high-vacuum mode with a Quanta 650 FEG scanning electron microscope (SEM) (FEI, Hillsboro, OR, USA) equipped with an Oxford Instruments X-Max<sup>N</sup> 150 mm energy-dispersive X-ray (EDX) detector (Oxford Instruments, Abingdon-on-Thames, UK) in combination with an Oxford Instruments Unity backscattered electron and X-ray (BEX) system (Oxford Instruments, Abingdon-on-Thames, UK) (Figure 3). AZtec 6.1<sup>TM</sup> BEX Mapping software was utilised to collect raw data and construct elemental maps; the parameters used during scanning are given in Table 1. AZtecFeature and AZtecMatch were

also tested to extract numerical data for individual grains and identify mineral phases within the HM suite, respectively.

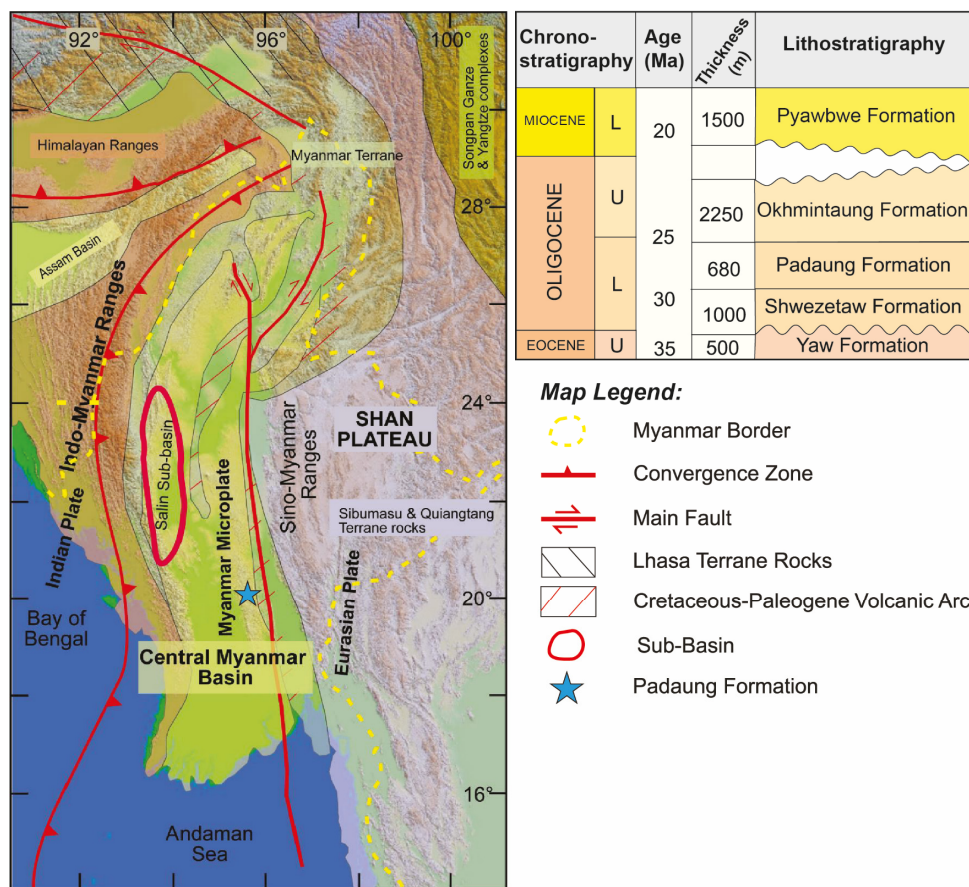


**Figure 1.** Digital elevation model (DEM) of Myanmar, showing the main geological terranes, alongside principal convergence zones and faults (left), alongside Oligocene lithostratigraphy of the Central Myanmar Basin, including the Padaung Formation (right). Modified from [29].

**Table 1.** Parameters used in mapping the surface of polished block and stub.

	Polished Block	Stub
Total number fields	164	84
Width per field (mm)	2.88	1.79
# pixels per field width	1024	1024
Montage pixel resolution	5560 × 5466	7413 × 7678
Scan time per field (s)	33	10
Magnification	145	233
Total scan time (h)	1.5	0.25
Dwell time (µs)	9.81	2.59
Operating voltage (kV)	20	20
Aperture strip position	1	1
Spot size	4.5	4.5
Working distance (mm)	9.6	10

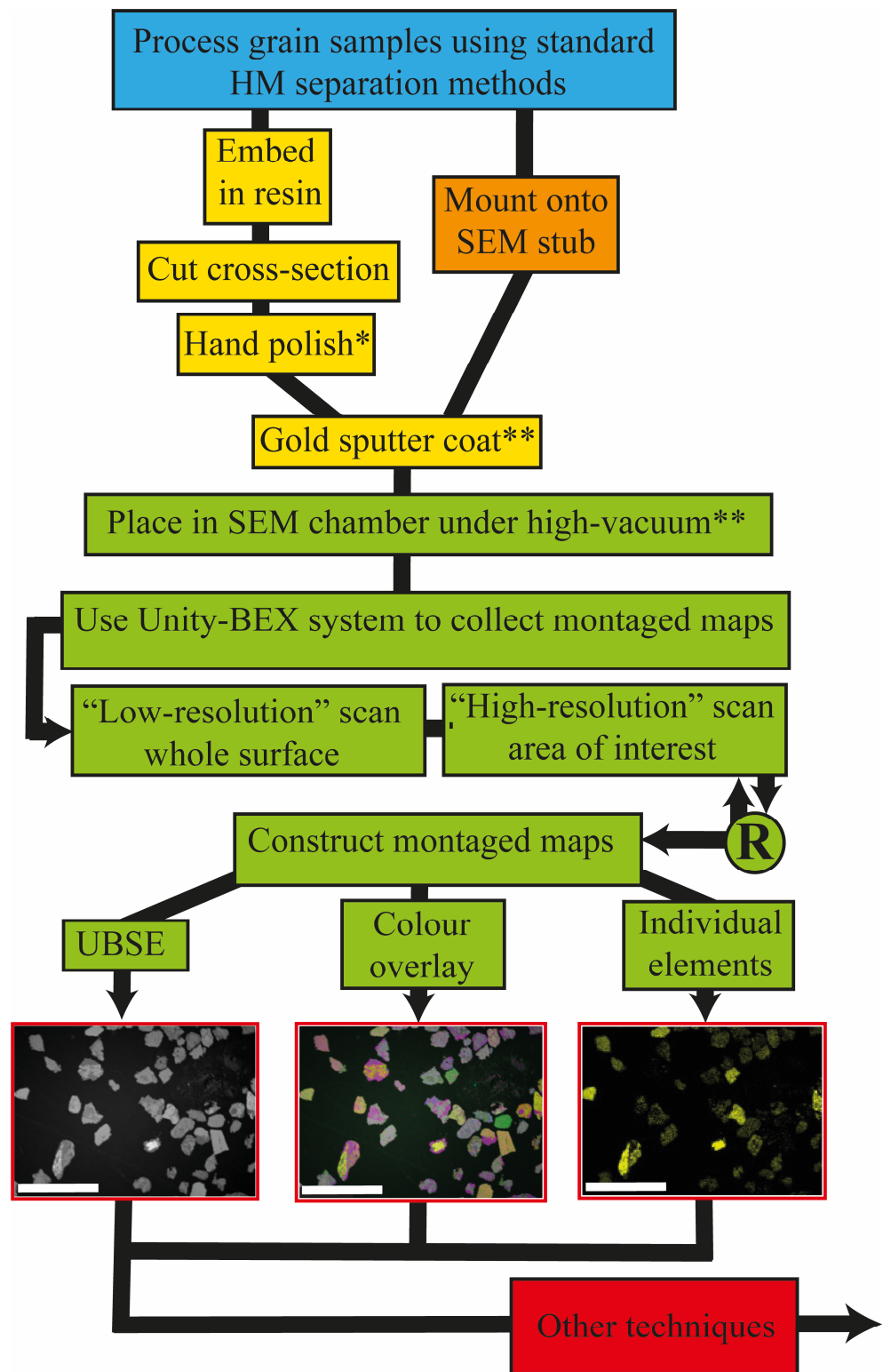


**Figure 2.** Schematic workflow of the methodology applied here. R = repeat if required. Red outlined boxes at the bottom of the workflow respectively illustrate the BSE image, composite layered map, and elemental map for Fe, all for the same location. \* Machine polishing will produce better images, but hand-polishing is adequate for most purposes. \*\* Samples can also be imaged and analysed under low-vacuum conditions (0.83 Torr), in which case no sputter coating is required. Solid red box indicates the potential for additional techniques (e.g., AZtecFeature, AZtecMatch, Raman microscopy, cathodoluminescence, in situ U-Pb geochronology, etc.).

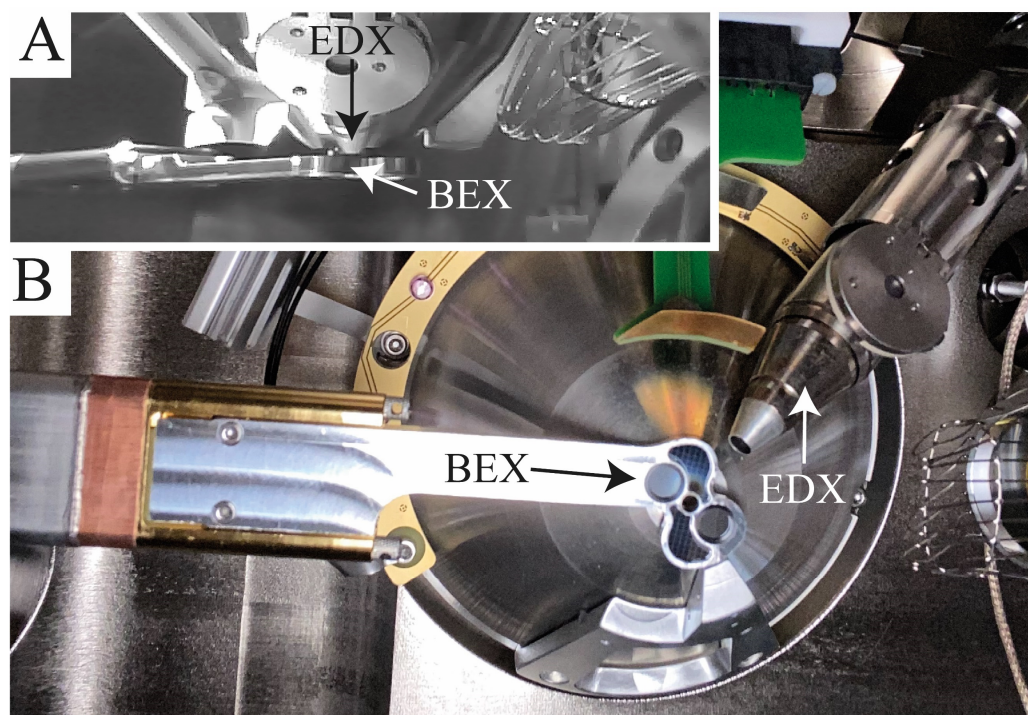


**Figure 3.** (A) Side view of relative position of the Unity BEX (BEX) detector and the X-Max<sup>N</sup> 150 mm detector (EDX) within the SEM chamber. (B) View of the underside of the SEM polepiece within the chamber, showing both BEX and EDX detectors.

### 3. Results

Both the polished block and stub were successfully scanned in a circular-shaped grid pattern (Figure 4A,B). In both cases, a range of grain types can be seen, illustrated by variations in the false-colour layered images produced by overlaying elemental data and backscattered (BSE) images (Figure 4). In addition, many grains are composite in nature (Figure 4C,D), and some particles have a complex interlocking texture (Figure 4D). Examples of elemental composition maps (Figure 5) collected from the polished block are shown for specific elements. From these, zircon grains can easily be identified from maps for Zr (Figure 5A). Identifying the occurrence and distribution of other indicative HM phases is also possible, including with titanite and rutile using iron and titanium maps (Figure 5B,C), for minerals high in calcium (Figure 5D) such as apatite and calcite, and for other silicate minerals using silica and aluminium maps (Figure 5E,F).

The collected elemental maps were imported into AZtecLAM (large area maps), where they were successfully differentiated into six separate phases (Figure 6A–F). These phases were further investigated with AZtecMatch. This uses a traffic light system to indicate the degree of confidence for any given match, with green representing a good match, yellow a more tentative suggestion, and red a low probability. Zircon, titanite, and apatite were automatically identified, showing good matches (green traffic light) with individually tested particles (Figure 7A–C). However, it should be noted that some particles in the third phase (Figure 6C) could also be calcite (green traffic light). The fourth phase (Figures 6D and 7D) was identified as epidote, but with less confidence (yellow traffic light), with other alternatives including andradite, grossular garnet, bytownite, lawsonite, anorthite, and zoisite/clinozoisite. The fifth and sixth phases were far less certain in their identification (red traffic light) with siderite, goethite, magnesium almandine (fifth phase, Figures 6E and 7E), and one possible olivine (fayalite, yellow traffic light), while the sixth phase was potentially identified as chromite (Figure 7F). The percentage coverage as part of the illustrated field of view (Figure 6A–F) was zircon = 0.11%, titanite = 4.73%, apatite = 0.89%, epidote = 15.23%, siderite = 0.55%, and chromite = 0.39%.

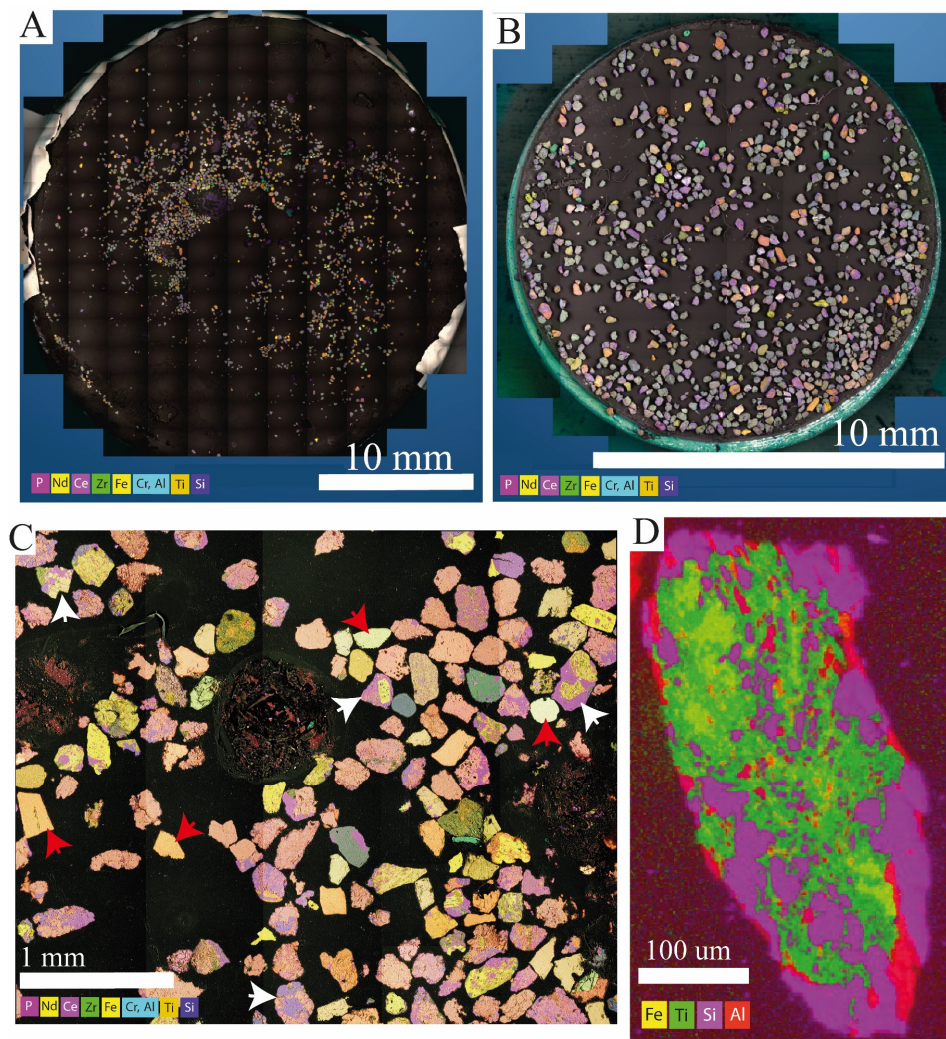


**Figure 4.** (A,B) stitched overview layered images of a polished block (A) and stub with natural grain surfaces (B). Images are a combination of backscattered (BSE) images and elemental maps for P, Nd, Ce, Zr, Fe, Cr, Al, Ti, and Si. (C) Zoomed image of area in (A), showing details of compositional variation within and between individual grains. Simple grains (red arrows), composite grains (white arrows). Composite grains with multiple phases indicate a degree of textural immaturity. Note that for all three images, colour variation indicates the occurrence of different mineral phases. (D) Detail of individual polished grain from (A), showing complex elemental distribution. Elemental spectrums can be further extracted from each grain or sub-areas within grains (see Figure 7).

AZtecFeature was successfully tested to extract physical information from a test area on the polished block (Figure 8), with representative numerical data for 20 grains presented here (Table 2). As shown, a range of useful data was extracted, which included the area, aspect ratio, breadth, length, equivalent circular diameter (ECD), perimeter, and shape (Table 2). Data also recorded the mean grey level of each individual particle and, in this case, a redundant measurement of grain orientation (direction, °). From the limited dataset, the aspect ratio and shape indicated a range of morphologies from equant rounded grains to elongated grains, with the size range of the exposed axes of these grains ranging from 24 to 242  $\mu\text{m}$ .

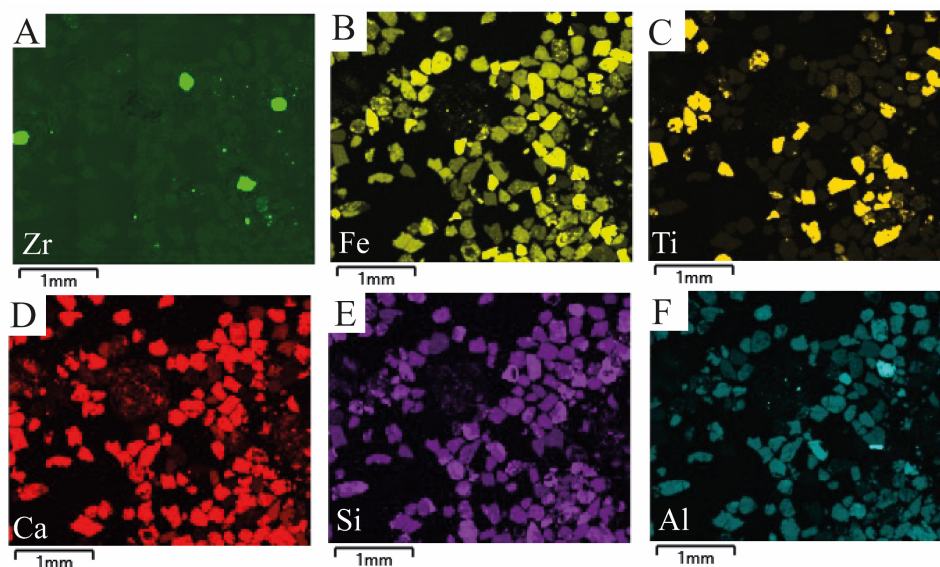


**Figure 5.** (A–F) Individual maps for the elements Zr, Fe, Ti, Ca, Si, and Al, respectively, from the area in Figure 4C. Note that Zr clearly indicates the occurrence of zircon, as does Ti for the presence of Ti-enriched phases, some of which also correlate with Fe bearing phases.

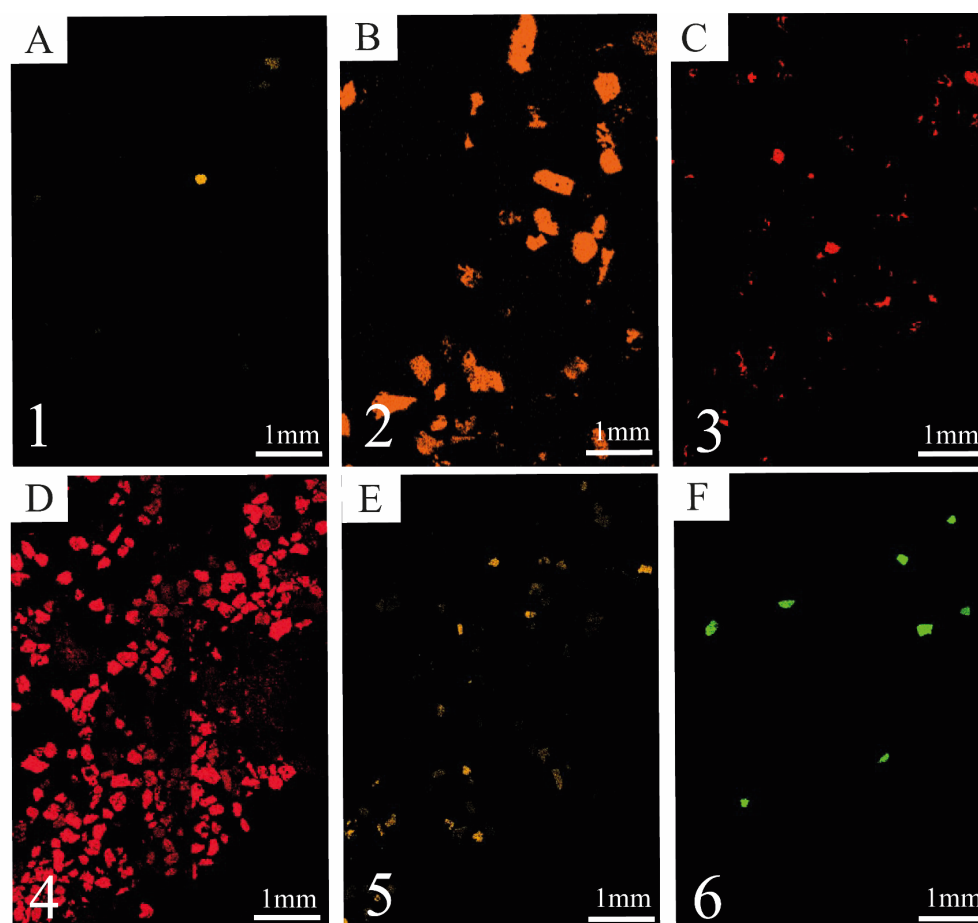


**Figure 6.** Elemental phase maps of selected area from polished block in Figure 4A. (A–F) Maps for six differentiated elemental phases (1–6) made using AZtecLAM (large area maps).

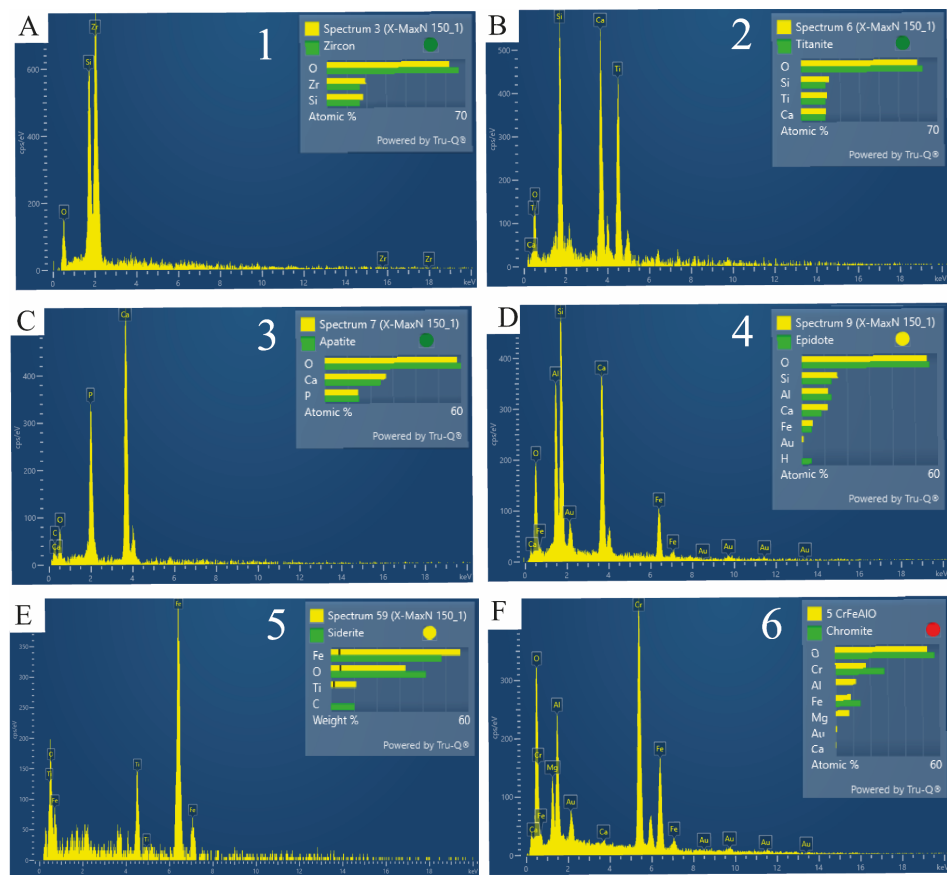


**Figure 7.** X-ray spectra, and identification of different mineral phases using AZtecMatch, from their corresponding elemental phase maps (Figure 6A–F). (A) zircon, (B) titanite, (C) apatite, and potentially (D) epidote, (E) siderite, and (F) chromite. Numbers refer to phase maps in Figure 6.

**Table 2.** Representative values recorded from 20 heavy mineral particles from the polished block, using AZtecFeature.

Area (µm <sup>2</sup> )	Aspect Ratio	Breadth (µm)	Direction (°)	ECD (µm)	Length (µm)	Mean Grey Level	Perimeter (µm)	Shape
1035	4	20	176	36	79	13,809	166	2
245	1	17	35	18	24	9824	64	1
2718	4	31	177	59	132	15,247	276	2
1343	3	31	8	41	80	12,253	190	2
2892	4	39	3	61	152	14,422	326	3
316	2	17	162	20	27	12,874	66	1
1027	2	31	158	36	61	14,641	136	1
1533	2	34	166	44	58	13,776	144	1
379	1	22	135	22	28	12,616	75	1
743	3	28	139	31	70	14,185	164	3
1446	1	39	38	43	54	11,803	143	1
6186	3	73	3	89	208	14,042	553	4
490	9	10	42	25	88	14,088	171	5
948	4	22	34	35	95	15,642	202	3
837	3	20	51	33	62	14,931	135	2
1991	2	42	121	50	66	12,733	167	1
14,316	3	96	3	135	242	17,370	572	2
1296	1	41	45	41	60	12,621	151	1
13,202	2	101	11	130	197	12,396	486	1
158	4	11	143	14	42	16,341	85	4

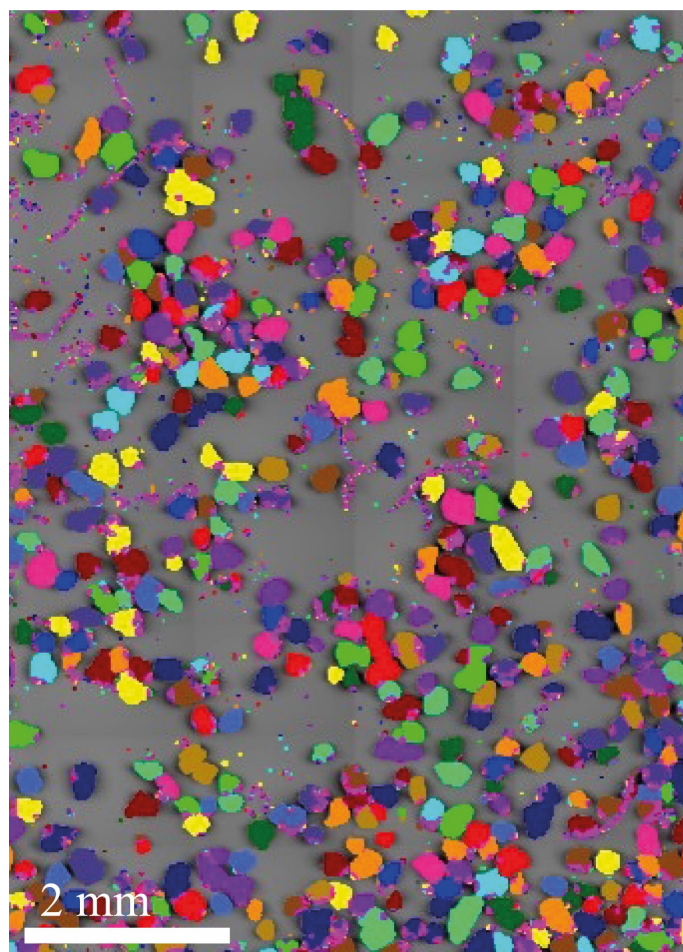


**Figure 8.** Selected area from stub sample, with grains highlighted to show separate features (particles) using AZtecFeature. The physical data (size, shape, aspect ratio, etc.) derived from these particles are shown in Table 2.

#### 4. Discussion

The Unity BEX system can be up to 100 times faster than existing EDX systems. In this study, the Unity BEX system was directly monitored, registering as 18 times faster than the installed X-Max<sup>N</sup> 150 mm EDX detector and recording an output rate in the region of 900 K cps. Other modern EDX detector systems may approach this improved analytical speed, especially in the case of multi-detector installations. However, improvements in the Unity BEX system are not limited to speed but also include the lack of shadowing artefacts in 3D grain mounts (Figure 9); significantly, it can be operated at a broader range of operational working distances (WD) and is not restricted to a single useable analytical WD.

The workflow shown here is ideal for the rapid location and distribution mapping of important mineral species such as zircon, apatite, titanite, and other heavy mineral phases. Zircon can be easily identified through maps of the element Zr, allowing for the possibility of later relocation for cathodoluminescence imaging (Figure 10), which is important for the recognition, imaging, and eventual dating of different growth zones [30]. Furthermore, if the resin mounting and machine polishing workflow (Figure 2) is followed, then this also allows for the in situ U-Pb geochronology of key minerals using LA-ICP-MS (e.g., zircon, apatite, titanite).

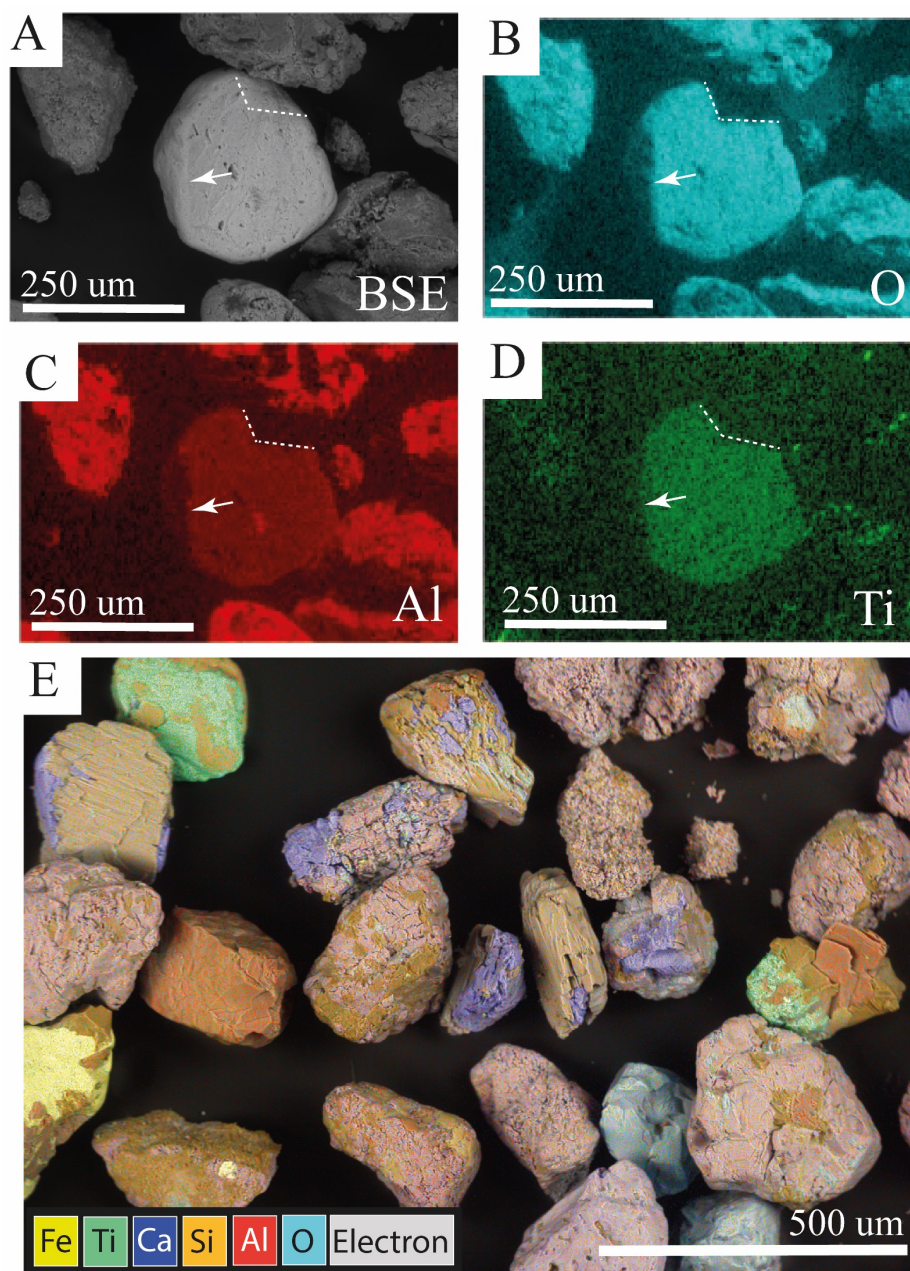


**Figure 9.** (A) BSE SEM image of grains on stub. (B–D) elemental maps for O, Al, and Ti over the same area as in (A). Note that (B–D) were taken using traditionally mounted X-Max<sup>N</sup> 150 mm EDX detector and, hence, show shadowing effects (dashed line and arrow) resulting in areas that have no X-ray signal. (E) Similar composite BSE/elemental image of grains on stub, but taken with Unity BEX detector, which does not exhibit shadowing artefacts due to the dual X-ray detectors placed at 180° to each other directly under the polepiece.

The combined backscattered electron and X-ray data produced by the Unity BEX also allow for the rapid identification of interlocking and complex chemical (mineralogical) textural relationships within single grains (Figure 4C,D). These complex chemical–textural relationships cannot be deconvolved using other mineral identification techniques (e.g., Raman spectroscopy [23]) and can be important for the interpretation of sediment maturity, which is dependent on the distance of transportation and the degree of weathering of HM suites or may indicate sedimentary recycling (e.g., lithic grains, surface corrosion, etc.) [3,5,6].

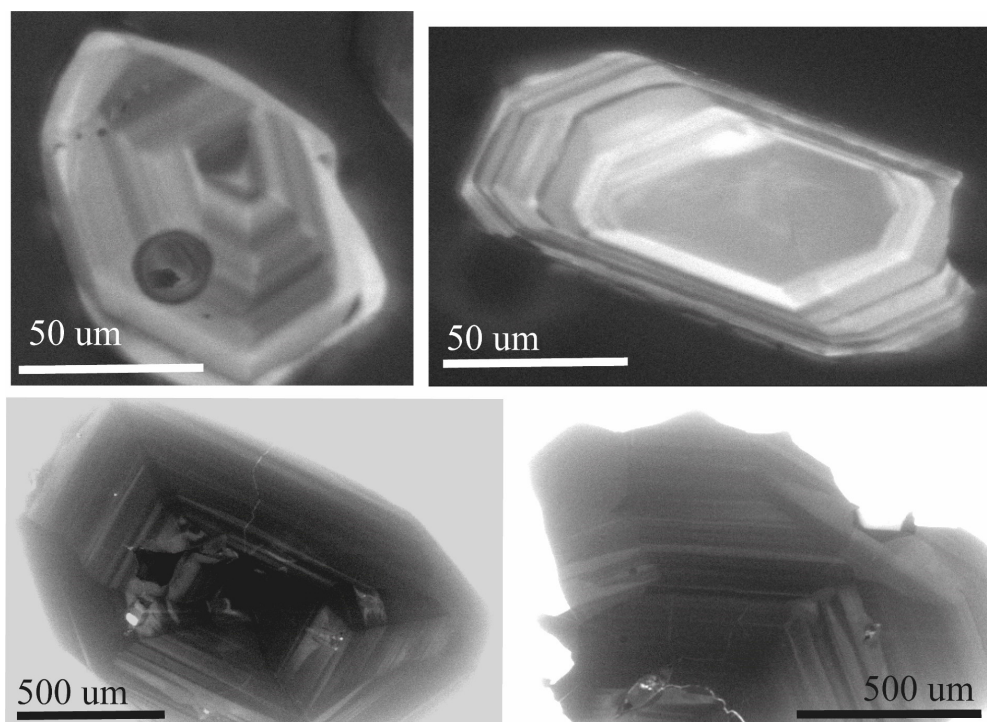


**Figure 10.** Typical SEM CL images of zircon, illustrating zones within the grains. Fast elemental mapping can be used to map out the locations of zircons (and other zoned mineral phases), allowing for further in situ analysis such as CL or U-Pb geochronology using LA-ICP-MS.

Despite these advantages in the rapid mapping and identification of heavy mineral phases, the Unity BEX system possess areas that require future optimisation. For example, the system cannot detect elements lighter than Na and can only produce qualitative results for the other elements. Light element analysis and full quantification can be achieved through integration with pre-existing standard EDX-type detectors, but this requires analysis to take place at a static working distance set for the EDX detector (e.g., 10 mm). In addition, results will vary depending on the type and age of the EDX detector partnered to the Unity BEX system. Newer and faster large-windowed EDX detectors will improve quantitative results, especially for lower atomic number elements (e.g., carbon and oxygen), and crucially allow for the reduction in scan times, increasing sample throughput without compromising on quality.

In addition, neither AZtecFeature nor AZtecMatch can currently take advantage of data derived through BEX and are restricted to utilising EDX spectral data, in this case from an X-Max<sup>N</sup> 150 mm detector system. For example, in AZtecFeature, although it is possible to threshold the BSE images obtained through BEX and, therefore, extract data on particle physical parameters (Table 2), it is not currently possible to utilise either BEX or EDX spectral data within the programme. In the case of AZtecMatch, it is possible to utilise the EDX data. However, the superior BEX spectra with higher count rates cannot be used for mineral matching.

The optimisation and integration of BEX spectra with AZtecMatch will be the key to developing automated heavy mineral identification using SEM-Unity BEX into a standard sedimentary provenance technique. Current quantitative techniques for automated heavy mineral identification such as Raman spectroscopy have been in use for a longer period and, as such, have well-developed and tested neural networks in place to identify a wider range of heavy minerals with high accuracy (e.g., [31]). A separate aliquot of the sample tested in this present study (MCM-18-004) has also been analysed using a Horiba XploRA Raman 532 μm laser coupled to an Olympus polarising microscope with a lens set at ×50 objective [32]. The heavy minerals assemblage identified using Raman spectroscopy shows

a dominance of epidote (58.4%) and garnet (13.6%). There are minor amounts of titanite (8.8%), amphibole (7.4%), apatite (3.9%), zircon (1.6%), and rutile (1.1%), along with a lower content of tourmaline (0.8%), chloritoid (0.6%), anatase (0.4%), chlorite (0.3%), and spinel (0.1%), with “Other” heavy minerals representing 3%.

The Unity BEX and AZtecMatch data and mineral identification presented here correlate well with this (Table 3), except for the abundant garnet signature (although it is noted that the abundant epidote can also be interpreted as magnesium almandine based on AZtecMatch data). Some of the differences may be due to the small sample size used for AZtecMatch. However, the complex interlocking nature of many of the grains, as well as the limitations of the factory library, have also influenced the results. It is worth noting that chromite from this present study may in part equate to spinel *sensu stricto*, as it also contains Mg and Al (Figure 7F). Separating forms of “spinel” is not easy, even with other techniques such as Raman spectroscopy (see [33]). Some material identified as chromite may, in part, also be garnet. In addition, the phase identified in AZtecMatch as siderite (yellow traffic light) may at least in part contain a proportion of a Ti-bearing mineral such as titanite, rutile, or anatase, as some EDX spectra contain up to 7 atomic% of Ti (Figure 7E). SEM-BEX is a powerful tool for rapid *in situ* mineral location and identification and provides crucial textural data that other techniques, such as Raman or QEMSCAN, cannot. However, the AZtecMatch database requires additional building and training to deconvolve complex heavy mineral assemblages fully.

**Table 3.** Comparison of heavy minerals observed by Raman spectroscopy and SEM-EDX for the same sample.

Mineral	Raman (%)	SEM-EDX *
Epidote	58.4	69.60
Garnet	13.6	
Titanite	8.8	21.62
Amphibole	7.4	
Apatite	3.9	4.07
Zircon	1.6	0.5
Rutile	1.1	2.51 †
Tourmaline	0.8	
Chloritoid	0.6	
Anatase	0.4	
Chlorite	0.3	
Spinel	0.1	1.78 ‡
Other HM	3	

\* note values from phases 1–6 normalised to 100%. † identified as siderite by AZtecMatch, but also contains up to 7 atomic% Ti. ‡ “Chromite” but with Mg and Al (spinel).

## 5. Future Workflow Optimisation

Based on the initial workflow development and testing of heavy mineral population identification using multiple analytical techniques (SEM-BEX and Raman spectroscopy), some recommendations can be made to improve future analysis.

The improved sample preparation and maximisation of particle concentration through the placement of multiple samples onto densely packed and machine-polished thin sections will increase productivity and data quality (Figure 11).

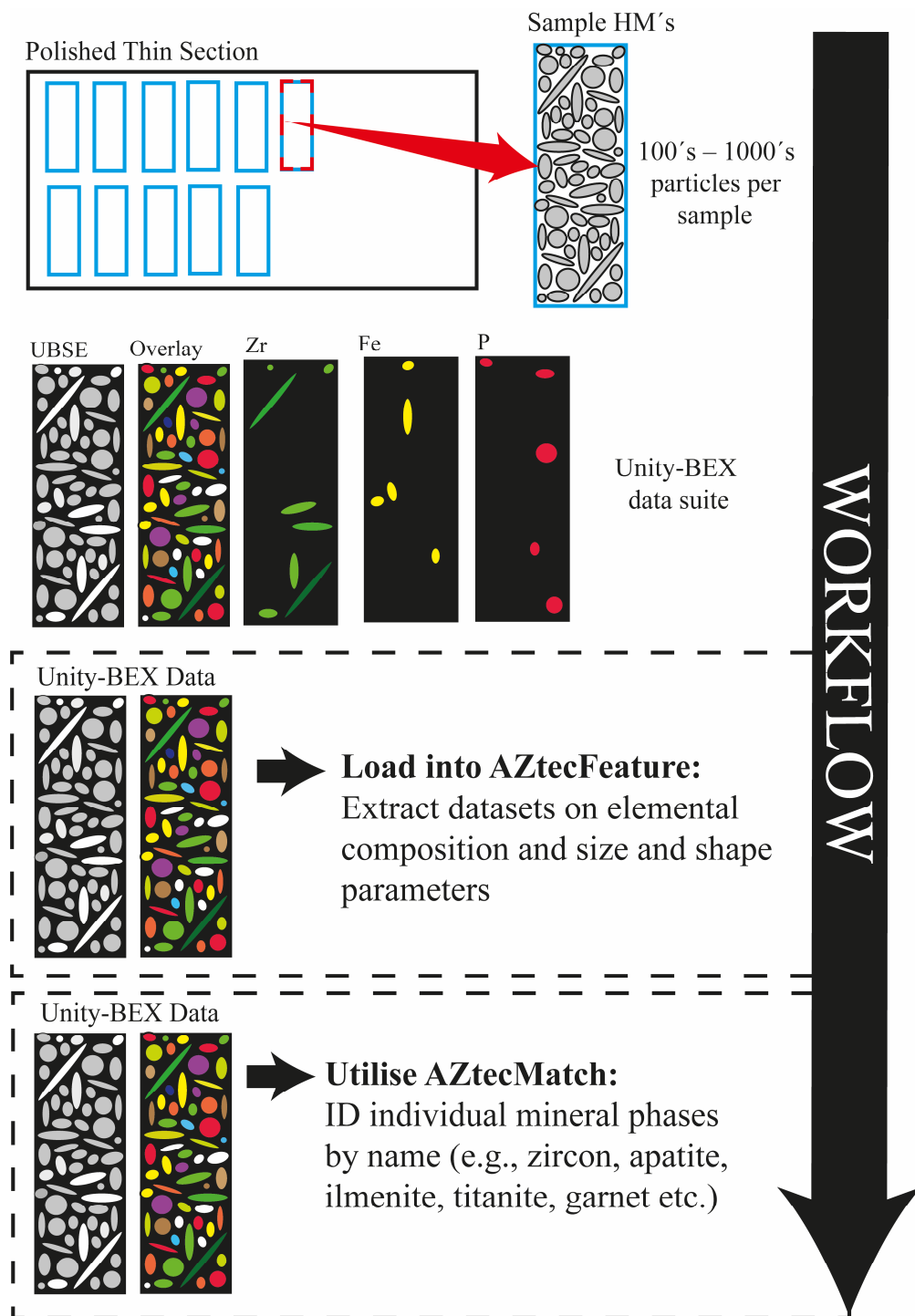


**Figure 11.** Future idealised workflow using subsets of heavy minerals on polished thin sections to increase efficiency in acquisition and implementation of phase identification. Note that the same workflow can equally be applied to grain mounts (unpolished samples). The workflow can also include other techniques such as Raman spectroscopy.

Fuller integration between the AZtec software options (i.e., BEX, AZtecFeature, AZtecMatch) and the integration of phase analysis from AZtecLAM into BEX would also greatly improve and optimise the workflows on heavy mineral suites. Therefore, some software development from Oxford Instruments would greatly improve usability and enhance semi-automated or automated interaction between the AZtec options (Figure 11). In the case of AZtecFeature, this would allow for the measurement of a range of shape and size

parameters (see example in Table 2), as well as the elemental spectral characterisation of each particle from Unity BEX maps. Such compatibility is possible between AZtecLAM and AZtecFeature but is not currently available under the Unity BEX analysis package. The combination of fast elemental mapping through Unity BEX, including on grain mounts, with comprehensive particle analysis would be particularly useful in the study of heavy minerals, as well as in other fields of investigation. The partial use of AZtecMatch herein, which could only utilise X-rays captured by the X-Max<sup>N</sup> 150 mm EDX detector, illustrates the potential to leverage the benefits of faster, more in-depth elemental data from Unity BEX. This would greatly benefit from full integration with AZtecMatch, allowing the construction of fast maps with particle analysis based on named mineral distributions.

AZtecMatch can utilise the user-defined libraries of mineral X-ray spectra. These can be collected under specific SEM conditions optimised for data collection (i.e., high-vacuum gold-coated, low-vacuum uncoated, High kV, low kV, etc.). The future development of such data libraries, specifically for heavy mineral suites, will help improve accuracy and allow better speciation of heavy mineral assemblages.

Recent developments in scanning electron microscopy (SEM) now allow for the integration of Raman spectroscopy within SEM. We highly recommend that this current proposed workflow (Figure 11) be modified to include an additional Raman spectroscopy step where appropriate.

## 6. Conclusions

This proposed workflow demonstrates that automated HM analysis using fast elemental X-ray mapping in conjunction with BSE imaging (Unity BEX) is practical and has the potential for the direct identification of mineral phases as well as the characterisation of several other physical parameters (size, shape, etc.) that are important for comprehensive provenance analysis. Further automation and integration of options within AZtec software (e.g., AZtecMatch) can only improve these possibilities. Such workflows are faster than traditional techniques that use optical microscopy or Raman spectroscopy, have the potential to be fully automated, and do not rely on the availability of personnel with specialist knowledge in heavy mineral grain identification.

**Author Contributions:** Conceptualization, J.B.; methodology, J.B.; formal analysis, J.B., A.G. and M.W.; resources, A.G., M.W. and J.B.; data curation, J.B. and A.G.; writing—original draft preparation, J.B., A.G. and M.W.; writing—review and editing, J.B., A.G. and M.W.; visualization, J.B. and M.W. All authors have read and agreed to the published version of the manuscript.

**Funding:** This research received no external funding.

**Data Availability Statement:** No data is available.

**Acknowledgments:** Royal Holloway University of London (RHUL) for use of heavy mineral separation facilities. Conor McMillan is thanked for collecting the sample used in this study. Scanning electron microscopy work was carried out at the Centre for Environmental Scanning Electron Microscopy (CESEM) at Heriot-Watt University (HWU).

**Conflicts of Interest:** The authors declare no conflicts of interest.

## References

1. Morton, A.C. Heavy minerals. In *Sedimentology Encyclopedia of Earth Science*; Springer: Berlin/Heidelberg, Germany, 1978. [[CrossRef](#)]
2. Morton, A.C. Heavy Minerals in Provenance Studies. In *Provenance of Arenites*; NATO ASI Series 148; Springer: Dordrecht, The Netherlands, 1985. [[CrossRef](#)]
3. Coll, X.; Gómez-Gras, D.; Roigé, M.; Teixell, A.; Boya, S.; Mestres, N. Heavy-mineral provenance signatures during the infill and uplift of a foreland basin: An example from the Jaca basin (Southern Pyrenees, Spain). *J. Sediment. Res.* **2021**, *90*, 1747–1769. [[CrossRef](#)]
4. Joshi, K.B.; Banerji, U.S.; Dubey, C.P.; Oliveira, E.P. Heavy minerals in provenance studies: An overview. *Arab. J. Geosci.* **2021**, *14*, 1330. [[CrossRef](#)]

5. Morton, A.C.; Smale, D. The effects of transport and weathering on heavy minerals from the Cascade River, New Zealand. *Sediment. Geol.* **1990**, *68*, 117–123. [[CrossRef](#)]
6. Sevastjanova, I.; Hall, R.; Alderton, D. A detrital heavy mineral viewpoint on sediment provenance and tropical weathering in SE Asia. *Sediment. Geol.* **2012**, *280*, 179–194. [[CrossRef](#)]
7. Morton, A.C.; Hallsworth, C.R. Identifying provenance-specific features of detrital heavy mineral assemblages in sandstones. *Sediment. Geol.* **1994**, *90*, 241–256. [[CrossRef](#)]
8. Morton, A.C.; Whitham, A.G.; Fanning, C.M. Provenance of Late Cretaceous to Paleocene submarine fan sandstones in the Norwegian Sea: Integration of heavy mineral, mineral chemical and zircon age data. *Sediment. Geol.* **2005**, *182*, 3–28. [[CrossRef](#)]
9. McNeil, J.D.; Gough, A.; Hall, R.; Lünsdorf, N.K.; Webb, M.; Feil, S. A multi-proxy provenance study of Eocene to Oligocene sandstones in the Salin Sub-basin, Myanmar. *J. Asian Earth Sci.* **2021**, *216*, 104825. [[CrossRef](#)]
10. Pickering, K.T.; Carter, A.; Andò, S.; Garzanti, E.; Limonta, M.; Vezzoli, G.; Milliken, K.L. Deciphering relationships between the Nicobar and Bengal submarine fans, Indian Ocean. *Earth Planet. Sci. Lett.* **2020**, *544*, 116329. [[CrossRef](#)]
11. Webb, M.; Gough, A.; Endinanda, F. Depositional environments and sedimentary provenance of the Cenozoic deposits of Natuna Island, Indonesia: Implications for basin evolution in central Sundaland. *Gondwana Res.* **2024**, *134*, 298–325. [[CrossRef](#)]
12. Wagner, G.A. Fission track dating of apatites. *Earth Planet. Sci. Lett.* **1968**, *4*, 411–415. [[CrossRef](#)]
13. Naeser, C.W.; Zimmermann, R.A.; Cebula, G.T. Fission-track dating of apatite and zircon: An interlaboratory comparison. *Nucl. Tracks* **1981**, *5*, 65–72. [[CrossRef](#)]
14. Lee, T.-H. SHRIMP U-Pb ages of the detrital zircons from the Cretaceous Ulyeonsan Formation, SE Korea: A small piece of stratigraphic correlation in eastern Asia. *Cretac. Res.* **2023**, *151*, 105626. [[CrossRef](#)]
15. Dung, N.T.; Bac, B.H.; An, D.M.; Anh, T.T.V. Distribution and Reserve Potential of Titanium-Zirconium Heavy Minerals in Quang an Area, Thua Thien Hue Province, Vietnam. In *Advances and Applications in Geospatial Technology and Earth Resources*; Bui, D.T., Do, A.N., Bui, H.-B., Hoang, N.-D., Eds.; Springer International Publishing: New York, NY, USA, 2018. [[CrossRef](#)]
16. Nzeh, N.S.; Popoola, P.; Okanigbe, D.; Adeosun, S.; Adeleke, A. Physical beneficiation of heavy minerals—Part 1: A state of the art literature review on gravity concentration techniques. *Heliyan* **2023**, *9*, e18919. [[CrossRef](#)] [[PubMed](#)]
17. Commeau, J.A.; Poppe, L.J.; Commeau, R.F. *Separation and Identification of the Silt-Sized Heavy-Mineral Fraction in Sediments*; U.S. Geological Survey Circular: Reston, VA, USA, 1991; Volume 1071.
18. Rahman, M.A.; Zaman, M.N.; Biswas, P.K.; Nandy, P.K. Physical separation for upgradation of valuable minerals: A study of sands of the Someswari river. *Bangladesh J. Sci. Ind. Res.* **2015**, *50*, 53–58. [[CrossRef](#)]
19. Andò, S. Gravimetric separation of Heavy Minerals in Sediments and Rocks. *Minerals* **2020**, *10*, 273. [[CrossRef](#)]
20. Andò, S.; Garzanti, E.; Padoan, M.; Limonta, M. Corrosion of heavy minerals during weathering and diagenesis: A catalogue for optical analysis. *Sediment. Geol.* **2012**, *280*, 165–178. [[CrossRef](#)]
21. Mounteney, I.; Burton, A.K.; Farrant, A.R.; Watts, M.J.; Kemp, S.J.; Cook, J.M. Heavy mineral analysis by ICP-AES a tool to aid sediment provenancing. *J. Geochem. Explor.* **2018**, *184*, 1–10. [[CrossRef](#)]
22. Le Pera, E.; Tangari, A.C.; Marinangeli, L.; Morrone, C.; Riber, R.; Andò, S. Provenance of modern sands from Baja California rivers (Mexico): Petrographic constraints from light and heavy minerals. *J. Sediment. Res.* **2023**, *93*, 617–641. [[CrossRef](#)]
23. Dunkl, I.; von Eynatten, H.; Andò, S.; Lünsdorf, K.; Morton, A.; Alexander, B.; Yoshida, K. Comparability of heavy mineral data—The first interlaboratory round robin test. *Earth Sci. Rev.* **2020**, *211*, 103210. [[CrossRef](#)]
24. Nie, J.S.; Peng, W.B. Automated SEM-EDS heavy mineral analysis reveals no provenance shift between glacial loess and interglacial paleosol on the Chinese Loess Plateau. *Aeolian Res.* **2014**, *13*, 71–75. [[CrossRef](#)]
25. Hao, H.; Guo, R.; Gu, Q.; Hu, X. Machine learning application to automatically classify heavy minerals in river sand by using SEM/EDS data. *Miner. Eng.* **2019**, *143*, 105899. [[CrossRef](#)]
26. Andò, S.; Garzanti, E. Raman spectroscopy in heavy-mineral studies. *Geol. Soc. Lond. Spec. Public.* **2014**, *386*, 395–412. [[CrossRef](#)]
27. Tangari, A.C.; Cirillo, D.; De Luca, R.; Miriello, D.; Pugliese, E.; Le Pera, E. Heavy Minerals Distribution and Provenance in Modern Beach and Fluvial Sands of the Betic Cordillera, Southern Spain. *Geosciences* **2024**, *14*, 208. [[CrossRef](#)]
28. Mange, M.A.; Maurer, H.F.W. *Heavy Minerals in Colour*; Springer Science & Business Media: Berlin/Heidelberg, Germany, 2012; p. 147. [[CrossRef](#)]
29. Gough, A.; Hall, R.; BouDagher-Fadel, M.K. Mid-Cenozoic fluvio-deltaic to marine environments of the Salin Sub-basin, Central Myanmar. *J. Asian Earth Sci.* **2020**, *190*, 104143. [[CrossRef](#)]
30. Corfu, F.; Hanchar, J.M.; Hoskin, P.W.; Kinny, P. Atlas of zircon textures. *Rev. Mineral. Geochem.* **2003**, *53*, 469–500. [[CrossRef](#)]
31. Lünsdorf, N.K.; Kalies, J.; Ahlers, P.; Dunkl, I.; von Eynatten, H. Semi-automated heavy-mineral analysis by Raman spectroscopy. *Minerals* **2019**, *9*, 385. [[CrossRef](#)]
32. McMillan, C. Sedimentary Provenance and Depositional Environments from the Oligocene Formations in the North of the Salin Sub-basin, Onshore Myanmar. Master's Thesis, Royal Holloway University of London, London, UK, 2019.
33. Zhang, L.; He, K.; Guo, Q. Spectroscopic Characteristics and Coloring Mechanisms of Different Colored Spinel from Myanmar. *Crystals* **2023**, *13*, 575. [[CrossRef](#)]

**Disclaimer/Publisher's Note:** The statements, opinions and data contained in all publications are solely those of the individual author(s) and contributor(s) and not of MDPI and/or the editor(s). MDPI and/or the editor(s) disclaim responsibility for any injury to people or property resulting from any ideas, methods, instructions or products referred to in the content.